Climate Sensitivity Estimated From Temperature Reconstructions of the Last Glacial Maximum

Andreas Schmittner,[1*] Nathan M. Urban,[2] Jeremy D. Shakun,[3] Natalie M. Mahowald,[4] Peter U. Clark,[5] Patrick J. Bartlein,[6] Alan C. Mix,[1] Antoni Rosell-Melé [7]

[1]College of Oceanic and Atmospheric Sciences, Oregon State University, Corvallis, OR 97331-5503, USA.

[2]Woodrow Wilson School of Public and International Affairs, Princeton University, NJ 08544, USA.

[3]Department of Earth and Planetary Sciences, Harvard University, Cambridge, MA 02138, USA.

[4]Department of Earth and Atmospheric Sciences, Cornell University, Ithaca, NY 14850, USA.

[5]Department of Geosciences, Oregon State University, Corvallis, OR 97331, USA.

[6]Department of Geography, University of Oregon, Eugene, OR 97403, USA.

[7]ICREA and Institute of Environmental Science and Technology, Universitat Autònoma de Barcelona, Bellarerra, Spain.

*To whom correspondence should be addressed. E-mail: aschmitt@coas.oregonstate.edu.

Assessing impacts of future anthropogenic carbon emissions is currently impeded by uncertainties in our knowledge of equilibrium climate sensitivity to atmospheric carbon dioxide doubling. Previous studies suggest 3 K as best estimate, 2–4.5 K as the 66% probability range, and non-zero probabilities for much higher values, the latter implying a small but significant chance of high-impact climate changes that would be difficult to avoid. Here, combining extensive sea and land surface temperature reconstructions from the Last Glacial Maximum with climate model simulations we estimate a lower median (2.3 K) and reduced uncertainty (1.7–2.6 K 66% probability). Assuming paleoclimatic constraints apply to the future as predicted by our model, these results imply lower probability of imminent extreme climatic change than previously thought.

Climate sensitivity is the change in global mean surface air temperature ΔSAT caused by an arbitrary perturbation ΔF (radiative forcing) of Earth's radiative balance at the top of the atmosphere with respect to a given reference state. The equilibrium climate sensitivity for a doubling of atmospheric carbon dioxide (CO_2) concentrations (ECS_{2xC}) from preindustrial times has been established as a well-defined standard measure (*1*). Moreover, because transient (disequilibrium) climate change and impacts on ecological and social systems typically scale with ECS_{2xC} it is a useful and important diagnostic in climate modeling (*1*). Initial estimates of ECS_{2xC} = 3±1.5 K suggested a large uncertainty (*2*), which has not been reduced in the last 32 years despite considerable efforts (*1-10*). On the contrary, many recent studies suggest a small but significant possibility of very high (up to 10 K and higher) values for ECS_{2xC} (*3-10*) implying extreme climate changes in the near future, which would be difficult to avoid. Efforts to use observations from the last 150 years to constrain the upper end of ECS_{2xC} have met with limited

success, largely because of uncertainties associated with aerosol forcing and ocean heat uptake (*8, 9*). Data from the Last Glacial Maximum (LGM, 19-23,000 years ago) are particularly useful to estimate ECS_{2xC} because large differences from pre-industrial climate and much lower atmospheric CO_2 concentrations (185 ppm versus 280 ppm pre-industrial) provide a favorable signal-to-noise ratio, both radiative forcings and surface temperatures are relatively well constrained from extensive paleoclimate reconstructions and modeling (*11-13*), and climate during the LGM was close to equilibrium, avoiding uncertainties associated with transient ocean heat uptake.

Here we combine a climate model of intermediate complexity with new syntheses of temperature reconstructions from the LGM to estimate ECS_{2xC} using a Bayesian statistical approach. LGM, $2\times CO_2$ and pre-industrial control simulations are integrated for 2000 years using an ensemble of 47 versions of the University of Victoria (UVic) climate model (*14*) with different climate sensitivities ranging from ECS_{2xC} = 0.3 to 8.3 K considering uncertainties in water vapor, lapse rate and cloud feedbacks on the outgoing infrared radiation (Fig. S1), as well as uncertainties in dust forcing and wind stress response. The LGM simulations include larger continental ice sheets, lower greenhouse gas concentrations, higher atmospheric dust levels (Fig. S2) and changes in the seasonal distribution of solar radiation (see SOM). We combine recent syntheses of global sea surface temperatures (SSTs) from the Multiproxy Approach for the Reconstruction of the Glacial Ocean (MARGO) project (*12*) and surface air temperatures over land based on pollen evidence (*13*), with additional data from ice sheets, land and ocean temperatures (28) (SOM; all reconstructions include error estimates Fig. S3). The combined dataset covers over 26% of Earth's surface (Fig. 1, top panel).

Figure 2 compares reconstructed zonally averaged surface temperatures with model

67 results. Models with ECS_{2xC} < 1.3 K underestimate the cooling at the LGM almost everywhere,
68 particularly at mid latitudes and over Antarctica, whereas models with ECS_{2xC} > 4.5 K
69 overestimate the cooling almost everywhere, particularly at low latitudes. High sensitivity
70 models (ECS_{2xC} > 6.3 K) show a runaway effect resulting in a completely ice-covered planet.
71 Once snow and ice cover reach a critical latitude, the positive ice-albedo feedback is larger than
72 the negative feedback due to reduced longwave radiation (Planck feedback), triggering an
73 irreversible transition (Fig. S4) (*15*). During the LGM Earth was covered by more ice and snow
74 than it is today, but continental ice sheets did not extend equatorward of ~40°N/S, and the tropics
75 and subtropics were ice free except at high altitudes. Our model thus suggests that large climate
76 sensitivities (ECS_{2xC} > 6 K) cannot be reconciled with paleoclimatic and geologic evidence, and
77 hence should be assigned near-zero probability.

78 Posterior probability density functions (PDFs) of the climate sensitivity are calculated by
79 Bayesian inference, using the likelihood of the observations ΔT_{obs} given the model
80 $\Delta T_{mod}(ECS_{2xC})$ at the locations of the observations. The two are assumed to be related by an error
81 term ε, $\Delta T_{obs} = \Delta T_{mod}(ECS_{2xC}) + \varepsilon$, which represents errors in both the model (endogenously
82 estimated separately for land and ocean) and the observations (Fig. S3), including spatial
83 autocorrelation. A Gaussian likelihood function and an autocorrelation length scale of λ = 2000
84 km are assumed. The choice of the autocorrelation length scale is motivated by the model
85 resolution and by residual analysis. See sections 5 and 6 in the SOM for a full description of the
86 statistical method, assumptions, and sensitivity tests.

87 The resulting PDF (Fig. 3), considering both land and ocean reconstructions, is multi-
88 modal and displays a broad maximum with a double peak between 2 and 2.6 K, smaller local

maxima around 2.8 K and 1.3 K and vanishing probabilities below 1 K and above 3.2 K. The distribution has its mean and median at 2.2 K and 2.3 K, respectively and its 66% and 90% cumulative probability intervals are 1.7–2.6 K, and 1.4–2.8 K, respectively. Using only ocean data the PDF changes little, shifting towards slightly lower values (mean 2.1 K, median 2.2 K, 66% 1.5 – 2.5 K, 90% 1.3 – 2.7 K), whereas using only land data leads to a much larger shift towards higher values (mean and median 3.4 K, 60% 2.8 – 4.1 K, 90% 2.2 – 4.6 K).

The best-fitting model (ECS_{2xC} = 2.4 K) reproduces well the reconstructed global mean cooling of 2.2 K (within two significant digits), as well as much of the meridional pattern of the zonally averaged temperature anomalies (correlation coefficient r = 0.8; Fig. 2). Significant discrepancies occur over Antarctica, where the model underestimates the observed cooling by almost 4 K, and between 45-50° in both hemispheres, where the model is also too warm. Simulated temperature changes over Antarctica show considerable spatial variations (Fig. 1), with larger cooling of more than 7 K over the West Antarctic Ice Sheet. The observations are located along a strong meridional gradient (Fig. S7). Zonally averaged cooling of air temperatures is about 7 K at 80°S, more consistent with the reconstructions than the simulated temperature change at the locations of the observations. Underestimated ice sheet height at these locations could be a reason for the bias (*16*), as could be deficiencies of the simple energy balance atmospheric model component, which may also be the reason for the large biases in the simulation of present day temperatures over Antarctica (not shown). Underestimated cooling at mid-latitudes for the best fitting model also points to systematic model problems, such as the neglect of wind or cloud changes.

Two-dimensional features in the reconstructions are less well reproduced by the model (r = 0.5; Fig. 1). Large-scale patterns that are qualitatively captured (Fig. 1) are stronger cooling

over land than over the oceans, and more cooling at mid to high latitudes (except for sea ice covered oceans), which is contrasted by less cooling in the central Pacific and over the southern hemisphere subtropical oceans. Continental cooling north of 40°N of 7.7 K predicted by the best-fitting model is consistent with the independent estimate of 8.3±1 K from inverse ice-sheet modeling (*17*).

Generally the model solution is much smoother than the reconstructions partly because of the simple diffusive energy balance atmospheric model component. The model does not simulate warmer surface temperatures anywhere, while the reconstructions show warming in the centers of the subtropical gyres, in parts of the northwest Pacific, Atlantic, and Alaska. It systematically underestimates cooling over land and overestimates cooling of the ocean (Fig. S8). The land-sea contrast, which is governed by less availability of water for evaporative cooling over land compared with the ocean (*18*), is therefore underestimated, consistent with the tension between the ECS_{2xC} inferred from ocean only versus land only data (Fig. 3). A possible reason for this bias could be overestimated sea-to-land water vapor transport in the LGM model simulations perhaps due to too high moisture diffusivities. Other model simplifications such as neglecting changes in wind velocities and clouds or errors in surface albedo changes in the dynamic vegetation model component could also contribute to the discrepancies. The ratio between land and sea temperature change in the best-fitting model is 1.2, which is lower than the modern ratio of 1.5 found in observations and modeling studies (*19*).

Despite these shortcomings, the best-fitting model is within the 1σ-error interval of the reconstructed temperature change in three quarters (75%, mostly over the oceans) of the global surface area covered by reconstructions (Fig. S8). The model provides data constrained estimates of global mean (including grid points not covered by data) cooling of near surface air

temperatures ΔSAT_{LGM} = –3.0 K (60% probability range [–2.1, –3.3], 90% [–1.7, –3.7]) and sea surface temperatures ΔSST_{LGM} = –1.7±1 K (60% [–1.1, –1.8], 90% [–0.9, –2.1]) during the LGM (including an increase of marine sea and air temperatures of 0.3 K and 0.47 K, respectively, due to 120 m sea-level lowering; otherwise ΔSAT_{LGM} = –3.3 K, ΔSST_{LGM} = –2.0 K).

The ranges of 66% and 90% cumulative probability intervals as well as the mean and median ECS_{2xC} values from our study are considerably lower than previous estimates. The most recent assessment report from the Intergovernmental Panel on Climate Change (*6*), for example, used a most likely value of 3.0 K and a likely range (66% probability) of 2–4.5 K, which was supported by other recent studies (*1, 20-23*).

We propose three possible reasons why our study yields lower estimates of ECS_{2xC} than previous work that also used LGM data. Firstly, the new reconstructions of LGM surface temperatures show less cooling than previous studies. Our best estimates for global mean (including grid points not covered by data) SAT and SST changes reported above are 30–40% smaller than previous estimates (*21, 23*). This is consistent with less cooling of tropical SSTs (–1.5 K, 30°S–30°N) in the new reconstruction (*12*) compared with previous datasets (–2.7 K) (*24*). Tropical Atlantic SSTs between 20°S–20°N are estimated to be only 2.4 K colder during the LGM in the new reconstruction compared to 3 K used in (*23*), explaining most of the difference between their higher estimates of ECS_{2xC} and ΔT_{LGM} (–5.9 K vs –3.5 K).

The second reason is limited spatial data coverage. A sensitivity test excluding data from the North Atlantic leads to more than 0.5 K lower ECS_{2xC} estimates (SOM section 7, Figs. S14, S15). This shows that systematic biases can result from ignoring data outside selected regions as done in previous studies (*22, 23*) and implies that global data coverage is important for

157 estimating ECS_{2xC}. Averaging over all grid points in our model leads to a higher global mean
158 temperature (SST over ocean, SAT over land) change (–2.6 K) than using only grid points where
159 paleo data are available (–2.2 K), suggesting that the existing dataset is still spatially biased
160 towards low latitudes and/or oceans. Increased spatial coverage of climate reconstructions is
161 therefore necessary in order to improve ECS_{2xC} estimates.

162 A third reason may be the neglect of dust radiative forcing in some previous LGM studies
163 (*21*) despite ample evidence from the paleoenvironmental record that dust levels where much
164 higher (*25, 26*). Sensitivity tests (Fig. 3, SOM section 7) show that dust forcing decreases the
165 median ECS_{2xC} by about 0.3 K.

166 Our estimated ECS_{2xC} uncertainty interval is rather narrow, < 1.5 K for the 90%
167 probability range, with most (~75%) of the probability mass between 2 and 3 K, which arises
168 mostly from the SST constraint. This sharpness may imply that LGM SSTs are a strong physical
169 constraint on ECS_{2xC}. However, it could also be attributable to overconfidence arising from
170 physical uncertainties not considered here, or from mis-specification of the statistical model.

171 To explore this, we conduct sensitivity experiments that perturb various physical and
172 statistical assumptions (Figs. 3, S14, S15). The experiments collectively favor sensitivities
173 between 1 and 3 K. However, we cannot exclude the possibility that the analysis is sensitive to
174 uncertainties or statistical assumptions not considered here, and the underestimated land/sea
175 contrast in the model, which leads to the difference between land and ocean based estimates of
176 ECS_{2xC}, remains an important caveat.

177 Our uncertainty analysis is not complete and does not explicitly consider uncertainties in
178 radiative forcing due to ice sheet extent or different vegetation distributions. Our limited model
179 ensemble does not scan the full parameter range, neglecting, for example, possible variations in

shortwave radiation due to clouds. Non-linear cloud feedbacks in different complex models make the relation between LGM and $2\times CO_2$ derived climate sensitivity more ambiguous than apparent in our simplified model ensemble (*27*). More work, in which these and other uncertainties are considered, will be required for a more complete assessment.

In summary, using a spatially extensive network of paleoclimate observations in combination with a climate model we find that climate sensitivities larger than 6 K are implausible, and that both the most likely value and the uncertainty range are smaller than previously thought. This demonstrates that paleoclimate data provide efficient constraints to reduce the uncertainty of future climate projections.

References

1. R. Knutti, G. C. Hegerl, *Nat Geosci* **1**, 735 (Nov, 2008).
2. J. G. Charney *et al.*, "Carbon Dioxide and Climate: A Scientific Assessment" (1979).
3. D. A. Stainforth *et al.*, *Nature* **433**, 403 (Jan 27, 2005).
4. G. H. Roe, *Science* **318**, 629 (10.1126/science.1144735, 2007).
5. D. L. Royer, R. A. Berner, J. Park, *Nature* **446**, 530 (Mar 29, 2007).
6. IPCC, *Climate Change 2007: The Physical Science Basis. Contribution of Working Group I to the Fourth Assessment Report of the Intergovernmental Panel on Climate Change*. S. Solomon *et al.*, Eds., (Cambridge University Press, Cambridge, United Kingdom, New York, NY, USA, 2007), pp. 996.
7. R. Knutti, T. F. Stocker, F. Joos, G. K. Plattner, *Clim Dynam* **21**, 257 (Sep, 2003).
8. C. E. Forest, P. H. Stone, A. P. Sokolov, *Tellus Series a-Dynamic Meteorology and Oceanography* **60**, 911 (Oct, 2008).
9. N. G. Andronova, M. E. Schlesinger, *Journal of Geophysical Research-Atmospheres* **106**, 22605 (Oct 16, 2001).
10. J. M. Gregory, R. J. Stouffer, S. C. B. Raper, P. A. Stott, N. A. Rayner, *J Climate* **15**, 3117 (Nov, 2002).
11. N. M. Mahowald *et al.*, *Journal of Geophysical Research-Atmospheres* **111**, D10202 (May 31, 2006).
12. MARGO Project Members, *Nat Geosci* **2**, 127 (Feb, 2009).
13. P. Bartlein *et al.*, *Clim Dynam* **37**, 775 (2011).
14. A. J. Weaver *et al.*, *Atmos Ocean* **39**, 361 (Dec, 2001).
15. M. I. Budyko, *Tellus* **21**, 611 (1969).
16. V. Masson-Delmotte *et al.*, *Clim Dynam* **26**, 513 (Apr, 2006).

17. R. Bintanja, R. S. W. van de Wal, J. Oerlemans, *Clim Dynam* **24**, 197 (Feb, 2005).
18. S. Manabe, M. J. Spelman, R. J. Stouffer, *J Climate* **5**, 105 (Feb, 1992).
19. R. T. Sutton, B. W. Dong, J. M. Gregory, *Geophys Res Lett* **34**, (Jan 16, 2007).
20. J. D. Annan, J. C. Hargreaves, *Geophys Res Lett* **33**, L06704 (2006).
21. J. Hansen *et al.*, *The Open Atmospheric Science Journal* **2**, 217 (2008).
22. D. W. Lea, *J Climate* **17**, 2170 (Jun, 2004).
23. T. Schneider von Deimling, H. Held, A. Ganopolski, S. Rahmstorf, *Clim Dynam* **27**, 149 (Aug, 2006).
24. A. P. Ballantyne, M. Lavine, T. J. Crowley, J. Liu, P. B. Baker, *Geophys Res Lett* **32**, L05712 (2005).
25. S. P. Harrison, K. E. Kohfeld, C. Roelandt, T. Claquin, *Earth-Science Reviews* **54**, 43 (Jun, 2001).
26. B. A. Maher *et al.*, *Earth-Science Reviews* **99**, 61 (2010).
27. M. Crucifix, *Geophys Res Lett* **33**, L18701 (Sep 19, 2006).
28. Data are available at the National Climatic Data Center at NOAA or at http://mgg.coas.oregonstate.edu/~andreas/data/schmittner11sci/index.html.

29. This work was supported by the Paleoclimate Program of the National Science Foundation through project PALEOVAR (06023950-ATM). Thanks to Sandy Harrison and two anonymous reviewers for thoughtful and constructive comments that led to significant improvements of the paper.

Figure Captions:

Figure 1. Annual mean surface temperature (sea surface temperature over oceans and near surface air temperature over land) change between the LGM and modern. Top: Reconstructions of sea surface temperatures from multiple proxies (*12*), surface air temperatures over land from pollen (*13*) and additional data (SOM). Bottom: Best-fitting model simulation (ECS_{2xC} = 2.4 K).

Figure 2. Zonally averaged surface temperature change between the LGM and modern. The black thick line denotes the climate reconstructions and grey shading the ±1, 2, and 3 K intervals around the observations. Modeled temperatures, averaged using only cells with reconstructions (see Fig. 1), are shown as colored lines labeled with the corresponding ECS_{2xC} values.

Figure 3. Marginal posterior probability distributions for ECS_{2xC}. Upper: estimated from land and ocean, land only, and ocean only temperature reconstructions using the standard assumptions (1 × dust, 0 × wind stress, 1 × sea level correction of ΔSST_{SL} = 0.32 K, see SOM). Lower: estimated under alternate assumptions about dust forcing, wind stress, and ΔSST_{SL} using land and ocean data.

Figures

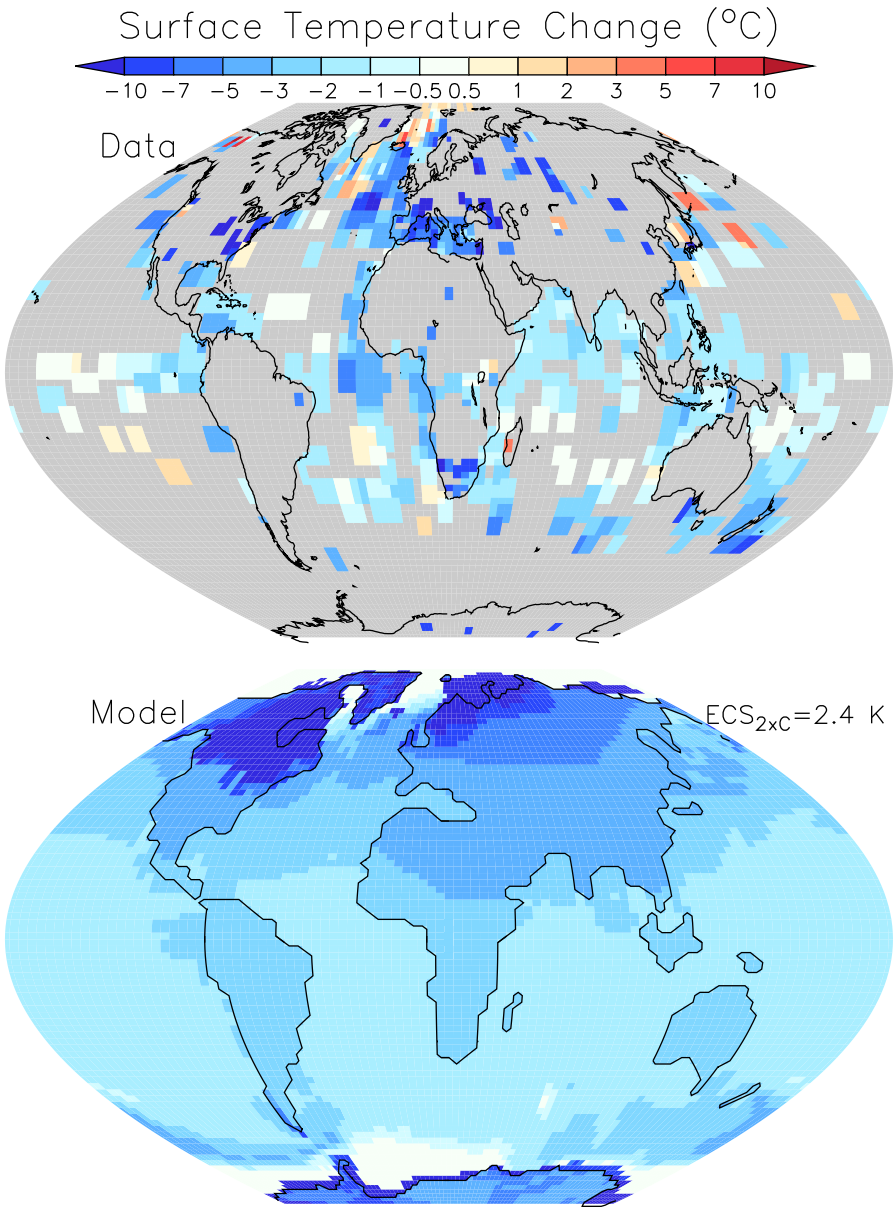

253

254 Figure 3. Annual mean surface temperature (sea surface temperature over oceans and near
255 surface air temperature over land) change between the LGM and modern. Top: Reconstructions
256 of sea surface temperatures from multiple proxies (*12*), surface air temperatures over land from
257 pollen (*13*) and additional data (SOM). Bottom: Best-fitting model simulation (ECS_{2xC} = 2.4 K).

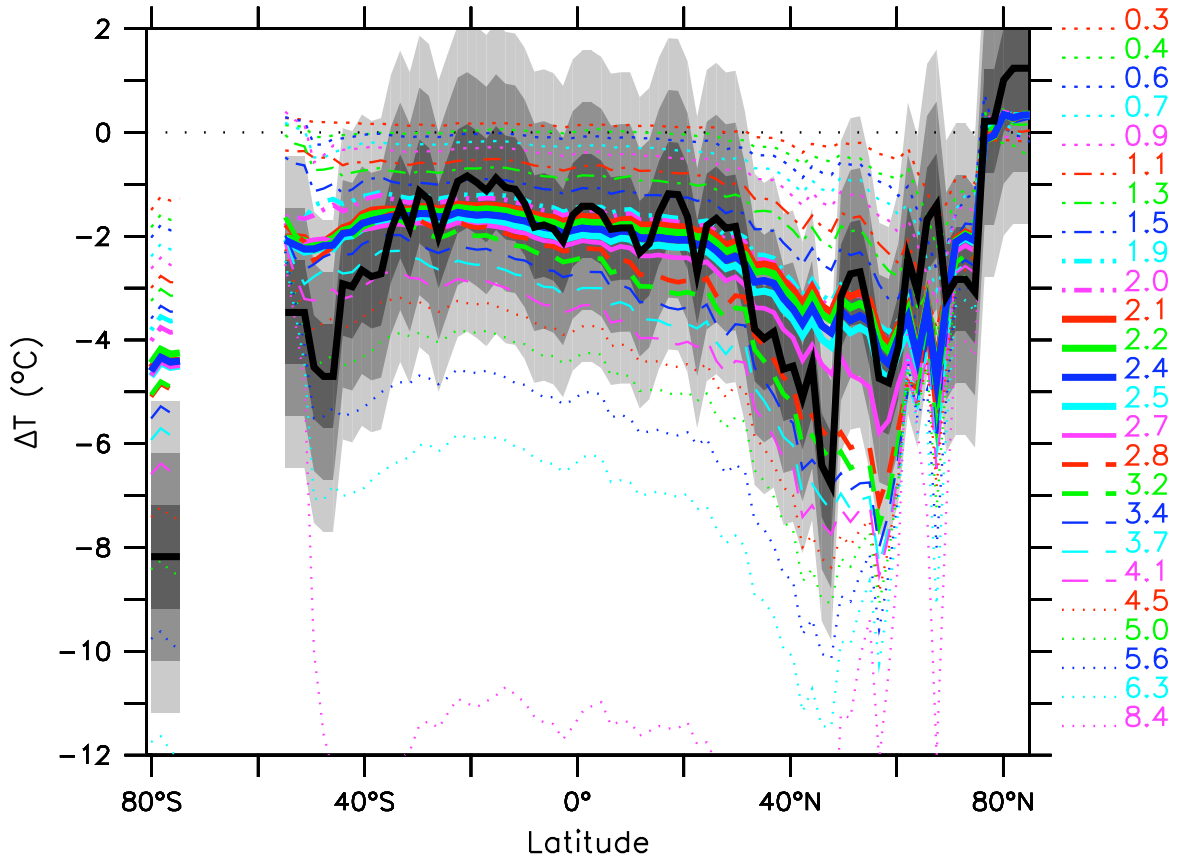

258

259 Figure 4. Zonally averaged surface temperature change between the LGM and modern. The
260 black thick line denotes the climate reconstructions and grey shading the ±1, 2, and 3 K intervals
261 around the observations. Modeled temperatures, averaged using only cells with reconstructions
262 (see Fig. 1), are shown as colored lines labeled with the corresponding ECS_{2xC} values.

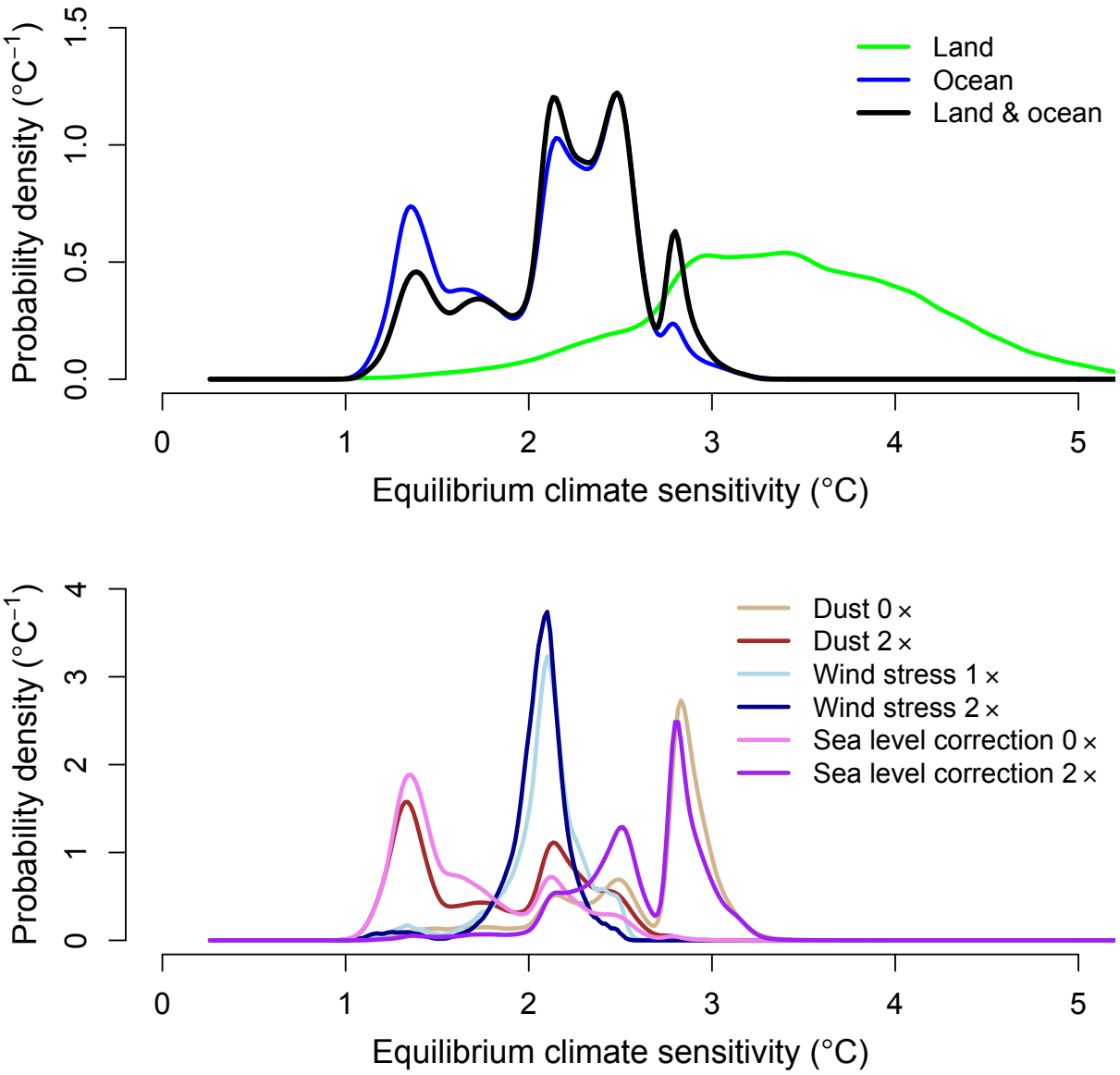

263
264 Figure 3. Marginal posterior probability distributions for ECS_{2xC}. Upper: estimated from land
265 and ocean, land only, and ocean only temperature reconstructions using the standard assumptions
266 (1 × dust, 0 × wind stress, 1 × sea level correction of ΔSST_{SL} = 0.32 K, see SOM). Lower:
267 estimated under alternate assumptions about dust forcing, wind stress, and ΔSST_{SL} using land
268 and ocean data.

269

270